

# Dimensionality Expansion of Load Monitoring Time Series and Transfer Learning for EMS

Blaž Bertalaníč, *Graduate Student Member, IEEE*, Jakob Jenko and Carolina Fortuna  
 Department of Communication Systems, Jožef Stefan Institute, Slovenia  
 {blaz.bertalanic, carolina.fortuna}@ijs.si

**Abstract**—Energy management systems (EMS) rely on (non)-intrusive load monitoring (NILM) to monitor and manage appliances and help residents be more energy efficient and thus more frugal. The robustness as well as the transfer potential of the most promising machine learning solutions for (N)ILM is not yet fully understood as they are trained and evaluated on relatively limited data. In this paper, we propose a new approach for load monitoring in building EMS based on dimensionality expansion of time series and transfer learning. We perform an extensive evaluation on 5 different low-frequency datasets. The proposed feature dimensionality expansion using video-like transformation and resource-aware deep learning architecture achieves an average weighted F1 score of 0.88 across the datasets with 29 appliances and is computationally more efficient compared to the state-of-the-art imaging methods. Investigating the proposed method for cross-dataset intra-domain transfer learning, we find that 1) our method performs with an average weighted F1 score of 0.80 while requiring 3-times fewer epochs for model training compared to the non-transfer approach, 2) can achieve an F1 score of 0.75 with only 230 data samples, and 3) our transfer approach outperforms the state-of-the-art in precision drop by up to 12 percentage points for unseen appliances.

**Index Terms**—feature dimensionality expansion, transfer learning, appliance classification, video-like transformation, Gramian angular field, deep learning, load monitoring.

## I. INTRODUCTION AND RELATED WORK

**I**NCREASED energy consumption that comes with population growth and technological advances raises environmental concerns globally. The European Union has committed to improving energy efficiency by at least 32.5% by 2030.<sup>1</sup> Next-generation power grids that allow bidirectional transmission of power and data, creating an automated power grid [1] are seen as one of the enablers of increased efficiency. Among other enablers are microgrids: small energy networks that includes some renewable energy generation units, such as photovoltaic panels, and some households. Both smartgrids and microgrids can operate within the existing power grid or in island mode, providing reliable power to connected households. Their flexible operation is enabled also by Energy Management Systems (EMS) [2], that have been shown to increase residential energy savings by more than 16% per year compared to traditional energy saving methods [3].

While EMS have been around for about four decades, they have been evolving both conceptually and technologically [3]. For instance, some studies show that only providing information about total energy consumption does not significantly

change consumers' energy consumption behavior, however, *when providing finer insights, such as into individual appliance consumption, energy saving behavior becomes noticeable* [4], [5]. As a result, future EMSs will likely include automatic monitoring and detection of household appliances to identify individual sources of energy consumption. Such capabilities are referred to in the domain as load monitoring and can be grouped into intrusive and non-intrusive techniques [6]. Intrusive Load Monitoring (ILM) assume that each electrical device operating in a building is connected to its own smart energy meter, possibly embedded in the electricity socket, that is subsequently connected to the EMS. Therefore, an ILM solution is more expensive as it requires more metering equipment, however more accurate as per device consumption data can be retrieved. For the case of Non-intrusive load monitoring (NILM), the entire energy consumption is monitored from a single central point in the building where a smart meter that connects to the EMS is installed. As a result, NILM provides a cheaper solution in terms of metering equipment and infrastructure maintenance thus being the preferred option as source of data for the EMS. However consumption data can only be collected in an aggregated form that need to then be processed to extract single device metering data.

### A. Related Work and Contribution

**Table I summarizes the most relevant state of the art with respect to NILM with the first column listing the authors and referencing the research. From the second column of the table, it can be seen that the state of the art approaches to solving NILM can be divided into three main types: regression/disaggregation, ON/OFF detection and appliance classification.**

*1) NILM problem type:* The regression problem focuses on decomposing the NILM signal into individual components, where each component represents a unique power signature for active appliances [7] as in the first row of Table I. The second type of problem studied refers to appliance ON/OFF classification [9], [10] as per rows two and three of the table. The motivation in these works is to identify whether or not a unique power signature represents an active device. It is important to note that the ON/OFF classification works assume the disaggregated signals are already available, thus the first type of problem is already solved. In some works, such as in rows four to six, the authors solve both type one and type two

<sup>1</sup>[https://ec.europa.eu/clima/eu-action/climate-strategies-targets/2030-climate-energy-framework\\_en](https://ec.europa.eu/clima/eu-action/climate-strategies-targets/2030-climate-energy-framework_en)

TABLE I  
SUMMARY OF THE RELATED WORK.

Work	Problem type	Approach		Dataset no.	Datasets (samp. freq.)	Device no.
		Input	DL mod.			
Zhang <i>et al.</i> [7]	Regression	TS	seq2point	2	REDD, UK-DALE (LF)	5
D’Incecco <i>et al.</i> [8]	Regression	TS	TL seq2point	3	REFIT, REDD, UK-DALE (LF)	5
Le <i>et al.</i> [9]	ON/OFF classification	TS	LSTM model	2	Own, AMPds (LF)	5
Le <i>et al.</i> [10]	ON/OFF classification	TS	RNN GRU	1	UK-DALE (LF)	up to 20
Kelly <i>et al.</i> [11]	Regress., ON/OFF class.	TS	Varying length AE	1	UK-DALE (LF)	5
Krystalakos <i>et al.</i> [12]	Regress., ON/OFF class.	TS	LSTM model	1	UK-DALE (LF)	5
Bonfigli <i>et al.</i> [13]	Regress., ON/OFF class.	TS	AE	3	AMPds, UK-DALE, REDD (LF)	up to 6
Zhou <i>et al.</i> [14]	Appliance class.	TS	TL LSTM	1	PLAID (HF)	6
Liu <i>et al.</i> [15]	Appliance class.	VI plot	TL CNN	2	PLAID, WHITED (HF)	11
De Baets <i>et al.</i> [16]	Appliance class.	VI plot	TL CNN	2	PLAID, WHITED (HF)	up to 22
<b>This work</b>	Appliance class.	sub-window GAF	CNN LSTM	5	UK-DALE, REDD, REFIT IAWE, ECO (LF)	up to 15

problems, i.e. disaggregation and ON/OFF classification [11], [12], [13]. Finally, the third type of problem is appliance classification listed in the last four lines of the table. This problem also assumes the disaggregated signals are available and aims to classify which device generated each unique power signature disaggregated from the NILM signal [15], [14], [16]. In this paper, *we focus on the appliance classification problem type*, where we assume that the signal is already disaggregated and therefore our work is intended to complement and build on regression approaches for disaggregation in the second step of NILM.

2) *Methods for solving NILM problems*: As the analysis of the related work shows, the approaches to solving the NILM involve a two stage process in which first a disaggregation step is required that is then followed by a classification step that performs either activity detection (i.e. ON/OFF classification), automatic appliance identification or both. It can also be seen from the second column of Table I that most research has focused on solving the regression/disaggregation and ON/OFF classification problem. Over the years, several methods have been proposed, some of which use combinatorics [17], thresholding [18], shallow machine learning such as Hidden Markov Models (HMM) [19], [20], [21], SVM [22], kNN [23], Naive Bayes, Logistic Regression Classifier and Decision Tree [24]. But as can be observed in the third column of Table I, most of the current state-of-the-art techniques are based on Deep Learning (DL) approaches such as recurrent neural networks (RNN)[11], [9], [25], [12], convolutional neural networks (CNN)[26], [11] and autoencoders (AE)[11], [13].

3) *NILM data for ML model training*: According to the last three columns of Table I, most of the regression/disaggregation and ON/OFF classification works employed a limited number of datasets and devices, with the exception of Le *et al.* [10], that used up to 20 devices. All the datasets used in these works are of low-frequency reflecting the actual real-world home meter deployments that tend to use low cost hardware. Also, most of the regression/disaggregation and ON/OFF classification approaches presented develop device-specific methods meaning that a separate DL model is trained for each device. As DL

models tend to work well when trained on more data, the generalization power of models trained with only a couple of datasets and relatively low number of samples per device may be limited.

According to the fifth column of Table I, the open-source NILM datasets used in the related state of the art were collected either with a low-frequency sampling (LF) [27], [28], [29], [30], [31], [32], [33] of 6 seconds or more or with a high-frequency sampling (HF) [34], [35] of 10000Hz or more. The fact that NILM techniques on LF data dominate in the studies summarized in the table may be related to the fact that the European Union and UK technical specifications for smart meters recommends a sampling rate of 10 seconds or less <sup>2</sup> for units installed in ordinary households.

However, as per Table I all the three appliance classification works have employed high-frequency datasets for model training, making the respective models less robust for already collected LF data measured with currently deployed smart meters. To avoid the necessity of buying and installing new HF smart meters and keep utilizing the existing ones whose readings are already accessible through the COSEM interface classes and OBIS Object Identification System <sup>3</sup>, we develop in this paper appliance classification and transfer models for existing LF meters that are directly compatible with the disaggregation works in lines 1-7 of the table in terms of sampling rate and complementary in their functionality.

4) *Time-series to image transformations for NILM*: Given the breakthroughs in image [36] and object recognition [37] in the last decade, various scientific fields have begun to formulate their domain-specific problems as image problems. Something similar happened in the NILM domain, where several time-series-to-image transformations that expand the 1D time series into a 2D image were considered. For example, [16], [15] transformed high-frequency datasets into a pixelated image of the voltage-current trajectory (VI) to solve the appliance classification

<sup>2</sup><https://ec.europa.eu/growth/tools-databases/tris/et/index.cfm/search/?trisaction=search.detail&year=2018&num=150&fLang=EN&dNum=1>

<sup>3</sup>[https://www.dlms.com/files/Blue\\_Book\\_Edition\\_13-Excerpt.pdf](https://www.dlms.com/files/Blue_Book_Edition_13-Excerpt.pdf)

problem. In [38], the authors proposed weighted recurrence graph plots on the same datasets for the same type of problem. Mottahedi *et al.* [39] were among the first to propose using Gramian Angular Filed (GAF) representation of NILM signals, solving the regression/disaggregation problem. Both [40] and [41] utilized the same transformation method and attempted to detect the ON/OFF state on a limited number of appliances. The computational complexity of TS to image transformations scales quadratically with the size of the TS window, so most of the listed works reduce the images by averaging them or alternatively choose a smaller window size to start with. The problem with averaging is that some of the information that may be important for solving the defined problem is lost, while choosing smaller window sizes may not capture enough information, resulting in poorer performance. In our work, we propose a new method for converting TS to a higher dimensional representation that scales linearly with the size of the TS window while preserving most of the information.

5) *Transfer learning for NILM*: According to lines 8-10 in Table I, the authors of [14], [15], [16] proposed the transfer learning (TL) method for appliance classification. Additionally, for the regression problem type it was shown by [8] that the use of a sequence-to-point DL model can be transferred between two different types of appliances for the regression/disaggregation problem, while [42] disaggregated signals using Generative Adversarial Networks and TL between houses in the same dataset. For appliance classification, both [15] and [16] proposed voltage-current trajectories representation of the signatures of devices on high-frequency data, while they used a convolutional neural network pre-trained on the ImageNet dataset for the backbone model. Their approach can be categorized as *cross-domain* TL. As shown by [43], *intra-domain* TL leads to better results than *cross-domain* TL in most cases. To the best of our knowledge our work is the first attempt at *intra-domain* TL for appliance classification on low-frequency datasets.

6) *Contributions*: Based on the presented related work it can be seen that in general there is a lack of research in NILM on appliance classification on low-frequency datasets, which is an important part in supporting disaggregation algorithms in correctly classifying the appliances based on their disaggregated signals in next generation EMS systems. In this paper, we propose a new approach for appliance classification in low frequency NILM, based on a time-series to sub-window image transformation and deep learning. The contributions of this paper are:

- We perform a first-time analysis of dimensionality expansion based representation for appliance identification and classification on low-frequency NILM signals.
- We introduce a *new dimensionality expansion* of time series signal through sub-window imaging, namely sub-window GAF, that scales linearly with the size of the TS window. Additionally, we improve upon the original GAF transformation by introducing brightness into the transformed images.
- We elaborate on the design methodology to develop a

new resource-aware deep neural network architecture for appliance classification on low-frequency NILM signals and extensively evaluate its performance on 5 *different* open datasets.

- We perform a first-time analysis of intra-domain transfer learning (energy domain to energy domain) on low-frequency data for appliance classification. We show that the proposed transfer learning (TL) approach performs with an average F1 score of 0.80, while requiring only a third of training epochs compared to training a model from scratch.
- We also perform a first-time analysis on how increase in number of samples and diversity of appliances affect the TL process.

This paper is organized as follows. Section II provides the formal problem statement, while Section III elaborates on the proposed time series transformation. Section IV introduces the proposed deep learning architecture, Section V describes the relevant methodological and experimental details, while Section VI provides thorough analyses of the results. Finally, Section VII concludes the paper.

## II. PROBLEM STATEMENT

Assume a new building **equipped with a LF smart meter that complies with the European Union and UK technical specifications for smart meters**<sup>4</sup> needs to be equipped with an EMS and connected to the smart grid as depicted on the left of Figure 1. Rather than collecting sufficient labeled data to deploy the appliance classification model in the EMS, we propose a new transfer learning (TL) approach for faster model development as depicted in the same figure. As can be seen in Figure 1a, there is a generic appliance classification model that has been trained on a larger already collected dataset, also referred to as the backbone model. This model is saved in the model storage. As depicted in Figure 1b, a relatively smaller number of labeled appliance data samples from the new house need to be collected and transformed to fine tune the pre-trained model loaded from the store before deploying it to the new EMS.

### A. Model development

In order to populate the model storage from Figure 1b with pre-trained models, appliance classification models need to be developed on sufficient data to achieve satisfactory performance. The required step-by-step training process is depicted in Figure 1a and formalized in Equation 1. Given an input tensor  $H_i$  representing energy measurements from households, that has been generated from raw TS measurements  $T_i$ , there is a function  $\Phi_i$  that maps the extracted features to a set of target classes  $C_i$  representing different household appliance types, where  $i$  denotes one of the datasets.

$$C_i = \Phi_i(H_i) \quad (1)$$

<sup>4</sup><https://ec.europa.eu/growth/tools-databases/tris/et/index.cfm/search/?trisaction=search.detail&year=2018&num=150&fLang=EN&dNum=1>

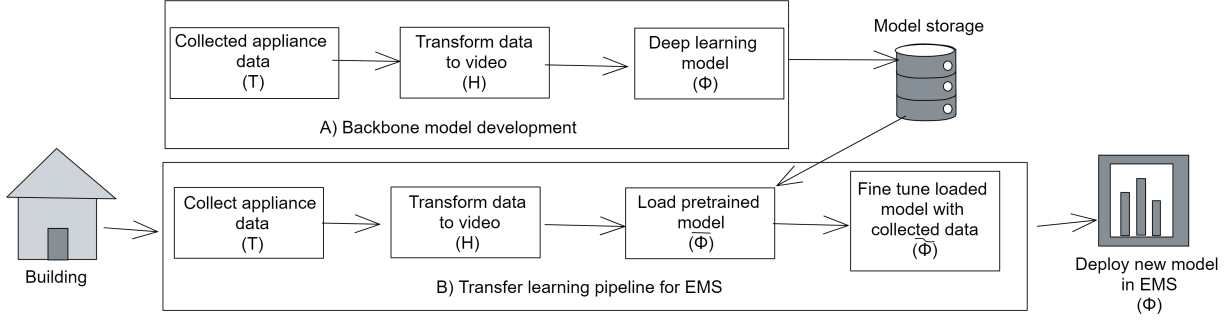


Fig. 1. Transfer learning enabled appliance classification model development for EMS.

The classifier  $\Phi_i$  is realized using one of the five different datasets to develop the deep learning model able to solve a multi-class classification problem to discriminate between the appliance classes within the selected datasets. The cardinality of the set  $C_i$ , also denoted as  $|C_i|$ , denotes the number of classes to be recognized, depending on the number of appliances present in the selected dataset.

### B. Model transfer

The classifier  $\Phi_i$  from Equation 1 can be decomposed into two parts: a backbone function  $\overline{\Phi}_i$  that extracts features from the input and a mapping function  $\widetilde{\Phi}_i$  that maps those features into the target classes as per Equation 2. This decomposition enables transferring the feature generation part to a new datasets as follows.

$$\Phi_i(H_i) = \widetilde{\Phi}_i(\overline{\Phi}_i(H_i)) \quad (2)$$

Given an input of  $H_j$ , that is generated by transforming a new time series  $T_j$ , there is a function  $\widetilde{\Phi}_j$ , that with the process of TL uses the output from the feature extraction function  $\overline{\Phi}_i$  from the function  $\Phi_i$ , trained on the  $i$ -th dataset, from the input  $H_j$ , and then maps it to a set of target classes  $C_j$  as depicted in Figure 1 and can be formalized as follows:

$$C_j = \widetilde{\Phi}_j(\overline{\Phi}_i(H_j)), i \neq j \quad (3)$$

The elements of  $C_j$  can be completely different or partially overlap with the ones of  $C_i$  and the cardinality  $|C_j|$ , represents the number of classes to be recognized, depending on the number of appliances in each dataset used in the TL process.

### III. FEATURE DIMENSIONALITY EXPANSION

We propose a new feature dimensionality expansion approach that converts time series data  $T$  into a video-like format represented as tensor  $H$  in Figure 1 as follows:

$$H_{(W \times W \times R)} = [F([T]_{(1 \times W)})]_{(R)}, \text{ where } R = \frac{N}{W} \text{ and } R \in \mathbb{N} \quad (4)$$

where function  $F()$  represents the transformation of the time series  $T$  into an image,  $N$  represents the length of the time-series,  $W$  represents the size of the sub-window and  $R$  represents the number of sub-windows. When  $W =$

$N$ ,  $F()$  is applied to the entire time series resulting in an image transformation such as the ones used in the state-of-the-art denoted by  $H_{(N \times N \times 1)}$ . When  $W = 1$ ,  $F()$  is applied to each point of the time series resulting in the original time-series  $H_{(1 \times 1 \times N)}$ . For all other values of  $W$ , the proposed transformation maps the input set of  $R$  time series of length  $W$  into  $R$  images of size  $W \times W$  resulting the video-like transformation denoted as  $H_{(W \times W \times R)}$ .

For realizing function  $F()$  from Eq. 4, we chose an amplitude aware GAF transformation. The standard GAF transformation may take one of two flavours: the Gramian angular summation field (GASF) or the Gramian angular difference field (GADF). In this work we chose to use the GASF representation because there was no difference in performance between the representations. For GASF, the time series needs to be scaled with a min-max normalization and then transformed to a polar coordinate system. The angles  $\phi_W$  from the polar plot are used to calculate the GASF therefore. The amplitude aware improvement that we proposed on the existing GAF transformation is to multiply every element of the GAF transformation with the maximum amplitude of the time series present in the sub-window. This introduces brightness into the transformed images that result in better model discrimination capabilities. The proposed  $F([T]_{(1 \times W)})$  is defined as:

$$F([T]_{(1 \times W)}) = \text{MAX}([T]_{(1 \times W)}) * \begin{pmatrix} \cos(\phi_W + \phi_1) & \cos(\phi_W + \phi_2) & \dots & \cos(\phi_W + \phi_W) \\ \vdots & \vdots & \ddots & \vdots \\ \cos(\phi_2 + \phi_1) & \cos(\phi_2 + \phi_2) & \dots & \cos(\phi_2 + \phi_W) \\ \cos(\phi_1 + \phi_1) & \cos(\phi_1 + \phi_2) & \dots & \cos(\phi_1 + \phi_W) \end{pmatrix} \quad (5)$$

The end result of consecutively applying  $F([T]_{(1 \times W)})$  from Eq. 5 to consecutive windows  $W$  is a sub-windowed GAF that is computationally less expensive compared to the original transformation. An example of the proposed transformation is depicted in the Figure 2. A TS of length  $N = 600$  depicted in Figure 2a is split into  $R = 5$  sub-windows of length  $W = 120$  as in Figure 2b. After applying the proposed transformation  $F()$  to the sub-windows a set of images of size  $M_R = 120 \times 120$  are concatenated as per Figure 2c forming one sample used for inference for appliance classification.

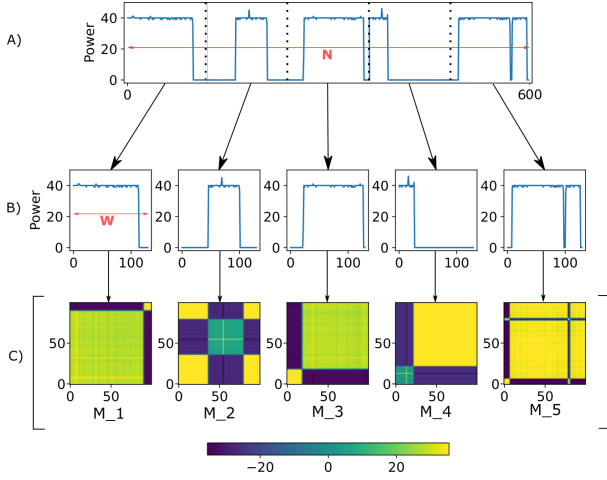


Fig. 2. Representation of the proposed method for time series sub-window and its GAF transformation.

#### IV. PROPOSED CLASSIFICATION MODELS

In this section we first describe the proposed model transfer that solved the problem from Section II a and then elaborate on the generic model development to be made available in the model store as discussed in Section II b.

##### A. Proposed video-like model

The proposed classification model, that will serve as the backbone as per Figure 1 for our TL model, is presented in Figure 3. Considering potential resource restrictions of BEMS, the backbone model was developed according to the design consideration guidelines presented in [44], making the model resource-aware by considering the amount of floating point operations (FLOPs) needed to make a prediction. In their work they proposed the following guidelines for model development:

a) *First guideline:* is to reduce the number of the layers of the network, by considering the number of layers  $L$  and the computational complexity of each individual layer  $F_l$  as per Eq. 6.

$$M_{FLOPs} = \sum_{l=1}^L F_l, \quad (6)$$

b) *Second is the optimization of the convolutional layers:* that represent a sequence of matrices used to extract features from the input image. The main part of the convolutional layer is a set of kernels of size  $K_r \times K_c$  used to convolve over an input tensor of size  $T_r \times T_c \times C$  with a stride  $S$ . The number of all FLOPs per filter  $F_{pf}$  is given by Eq. 7.

$$F_{pf} = \left( \frac{T_r - K_r + 2P_r}{S_r} + 1 \right) \left( \frac{T_c - K_c + 2P_c}{S_c} + 1 \right) (CK_r K_c + 1) \quad (7)$$

The first bracket of the equation gives the height of the output tensor, where  $T_r$  represents the number of the input rows, while  $K_r$  is the number of the filter rows,  $P_r$  is the row padding and  $S_r$  is the row stride size. The second

bracket represents the same calculation for the width of the output tensor, where the variables  $T_c$ ,  $K_c$ ,  $P_c$  and  $S_c$  correspond to the columns. The last bracket represents the number of computations per filter for each of the input channels  $C$ , which can also be considered as the depth of the input tensor and the bias. The number of FLOPs in the convolutional layer is equal to the number of filters times the FLOPs per filter given in Eq. 7, i.e.  $F_c = (F_{pf} + N_{ipf})N_f$ . However, in the case of using ReLU, an additional comparison and multiplication are required to calculate the number of FLOPs  $F_{pe}$  used in an epoch. We therefore added the number of FLOPs used for each filter and the number of instances for each filter and then multiplied by the number of all filters  $N_f$ :

$$F_c = (F_{pf} + (2CK_r K_c + 1))N_f. \quad (8)$$

c) *The third optimization to consider is the number of LSTM layers and hidden nodes within each:* According to the corresponding equation from [45] where  $T$  is the input tensor into LSTM layer and  $N_n$  is the number of hidden units, additionally the equation is multiplied by 4 because an LSTM has 3 gates and 1 memory cell, and by 2 because each weight value causes a multiply-and-addition operation.

$$F_{lstm} = (T + N_n) \times N_n \times 4 \times 2. \quad (9)$$

Finally, to compute the FLOPs of Fully Connected (Dense) layers the following equation is utilized:

$$F_{fc} = 2T \times O + O \quad (10)$$

The number of operations depends on both the input size  $T$  and the output size  $O$ , where  $O$  equals the number of nodes selected in the Dense layer.

During our iteration process we considered:

- The number of convolutional layers  $L_{cnn} \in \{2, 3, \dots, 24\}$
- The number of LSTM layers  $L_{lstm} \in \{1, 2, \dots, 10\}$ , with number of nodes  $N_N \in \{8, 16, 24, \dots, 128\}$

Based on the guidelines and empirical experimentation, the following model was selected since it provided the best ratio between the number of FLOPs and performance of the model. The input sequence of images is first fed into the feature extraction part of the model ( $\Phi$ ), that consist of convolution layer with 16 kernels of size  $7 \times 7$ , followed by a max pooling layer with pooling size of  $2 \times 2$ . Next come two similar blocks where each block consists of two convolution layers with 16 kernels of size  $3 \times 3$  and max pooling layer with pooling size of  $2 \times 2$ . The last part of the model starts with a dropout layer of 0.1, followed by two more convolution layers with the same kernel number and size as the previous layers. All of the mentioned convolution layers use 'same' padding and stride of 1 and use ReLU activation function, while being embedded into the TimeDistributed class from Keras library<sup>5</sup>. The output data from the convolutional part of the model is then flattened and fed into two LSTM layers with 16 nodes which are also the final two layers of the feature extraction

<sup>5</sup>[https://keras.io/api/layers/recurrent\\_layers/time\\_distributed/](https://keras.io/api/layers/recurrent_layers/time_distributed/)

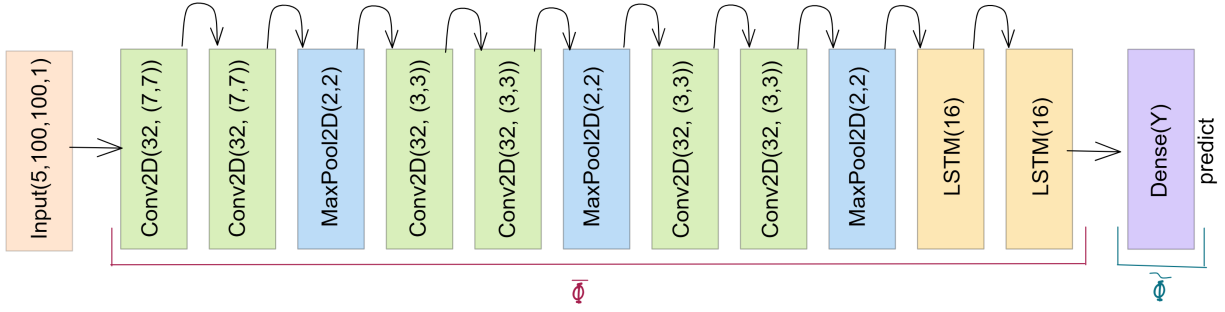


Fig. 3. Deep learning network model for NILM classification

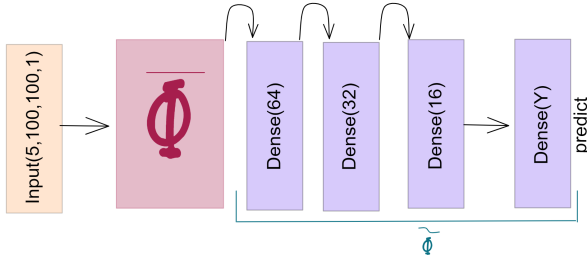


Fig. 4. Deep learning network model for TL NILM classification

part ( $\bar{\Phi}$ ), of the model. This output is then connected to the classification part ( $\hat{\Phi}$ ), of the model consisting of only one output layer of size  $Y$ , where the softmax activation function is applied and the classification is made. The size of  $Y$  depends on the number of different classes present in the used dataset. **Considering an input shape of  $5 \times 100 \times 100$  the final FLOPs computation for this proposed model sums up to  $\approx 2.92$  GFLOPs as listed in the first line of Table II.**

TABLE II  
MODEL FLOPs COMPARISON.

Input	Model	GFLOPs
Sub-windowed GAF	<b>Proposed model</b>	$\approx 2.92$
GAF	State of the art VGG11	$\approx 13.3$
TS	State of the art FCN	$\approx 0.14$
TS	State of the art ResNet	$\approx 0.27$
Sub-windowed GAF	<b>Proposed TL model</b>	$\approx 2.92$

1) *State of the art image-like model:* To compare how the proposed model fairs against other dimensionality expansion models an image-like model was developed. A series of well know DL architectures were considered in the evaluation and the one with the best performance was selected. AlexNet [36] and VGG11 to VGG16 [46] were all evaluated, due to their similarity to our proposed model, and in the end VGG11 performed the best out of all the evaluated architectures and was selected as baseline model.

The data was sliced into 60 minute long windows and each window was then transformed into Gramian angular summation field (GASF) image. Since the average 60 minute sample of time series transformed into images contains up

to 600 samples, a direct transformation would produce larger images of size  $600 \times 600 \times 1$  pixels, which require substantial computational power to train. **Due to hardware limitations we reduce the size of the input, similar approach was used in other related works as discussed in Section I-A4.** A rolling averaging process is applied to the time series that reduces its size to 300 samples, which are then converted to images of size  $300 \times 300$  pixels. The final number of FLOPs required for inference of the VGG11 model used is 13.3 GFLOPs, as can be seen in the second line of Table II.

2) *Baseline time series model:* To ensure the necessity of transforming TS through the proposed dimensionality expansion techniques, a comparison was made with the raw TS deep learning models. Two state of the art deep learning architectures that were shown to have excellent performance on the standard time series benchmarks consisting of 128 datasets [47] were selected: Fully Convolutional Network (FCN) and a modified version of ResNet both proposed by Wang *et al.* [48]. Each dataset was sliced into 60 minute long windows which ideally resulted in 600 samples per time series window. Since we were working with real world data and there might be missing values a moving average was applied to each sample, resulting in the reduced number of samples per TS window of 550, which was also the size of the input into both raw TS benchmark models, while being consistent with the proposed model. The computational complexity of both models is presented in the third and fourth line in Table II and shows that the ResNet model with  $\approx 0.27$  GFLOPs is almost two times more expensive to compute than the FCN model with  $\approx 0.14$  GFLOPs. However, both models are significantly less expensive compared to the imaging model VGG11 and our proposed model.

### B. Proposed model transfer

For realizing the transfer from an existing model to a new BEMS, we propose the TL model depicted in Figure 4. The feature extraction part ( $\bar{\Phi}$ ) is obtained from a model available in the model store as depicted in Figure 1. The backbone model is frozen and is not fine tuned during the training process. The features extracted from the backbone are provided as an input to the classification part ( $\hat{\Phi}$ ) of the model that includes three dense layers, first consisting of 64 nodes, second of 32 nodes while the third has 16 nodes.

All three dense layers use the ReLU activation function. The output from the last dense layer is then fed into the final output layer of size  $Y$ , where the final classification is made after the softmax activation function is applied. The size  $Y$  depends on the number of different appliances available in the new household. The number of additional dense layers was selected based on a trial and error iterative approach. During the iterative process we considered:

- The number of additional dense layers  $N_L \in \{1, 2, \dots, 10\}$
- The number of nodes in additional dense layers  $N_N \in \{8, 16, 24, \dots, 256\}$

The final number of  $N_L$  and  $N_N$  was chosen as a performance to resource awareness trade-off. **The model complexity can be seen in the last line of Table II with  $\approx 2.92$  GFLOPs. Although additional layers were added they did not significantly raise the number of FLOPs compared to the backbone model.**

## V. METHODOLOGY AND EXPERIMENTAL DETAILS

To present experiment details of our work we first describe the dataset generation procedure and then present details of the model training and results evaluation.

### A. Training data preparation

For this study, we selected datasets that are sufficiently large in terms of appliance count and per-appliance measurements while also being public, accepted in the community and be representative of power consumption across different continents. The five sets are UK-DALE[27], ECO [28], REDD [29], IAWA[30] and REFIT [31]. The traces were preprocessed with the NILMTK toolkit [49] that also filters bad sectors from the data and then split into windows  $W$  and sub-windows  $N$  and transformed into GASF images.

Table III provides a summary of the five datasets. The first column shows the dataset name, the second provides the sampling frequency used for collecting the data, while the third column shows the time period over which the samples were collected. It can be seen that all sampling rates have comparable frequency between 1 and 8 s, IAWA collection span is only 73 days while UK-DALE covers more than 4 years. To convert the TS to video-like format as discussed in Section III, the data first had to be resampled to synchronize the sampling rates of the different datasets. UK-DALE was chosen with a sampling rate of 6 seconds between each sample, which resulted in a round number of 10 samples per minute. Next, the data was split into sub-intervals with a fixed window length.

**The sub-window length  $W$  was determined based on the empirical testing so that the best ratio between the number of FLOPs and performance results was obtained. Through the experiments we determined that a TS window length  $W$  of 65 minutes that produced  $R = 5$  sub-windows of length of 13 minutes was the best at capturing appliances operational time. This ideally resulted in  $W = 130$  samples per sub-window. Only positive samples with activity were selected for the training dataset. Based on the analysis of all the selected datasets we determined that a device**

**is active if the maximum measured value within the TS window was at least 20W. Since we were dealing with the real world data measurements there could be some missing data within the sub-interval due to the data collection process. This would force us to discard a significant portion of the datasets and also some of the selected appliances. So to compensate for the possible missing values in the interval, moving average was used to reduce the number of samples within a sub-window. Although, this led to a small loss of information, through experiments we observed that the performance drop was not significant in comparison to the averaged datasets, additionally also lowering the computational complexity of the model.**

The forth column shows how many different houses were monitored and the fifth column gives information on how many different appliances were measured. It can be seen that IAWA only contains data from one house with 9 appliances, UK-DALE contains 5 houses and 53 appliances while REFIT includes 20 houses and 23 appliances. Columns 6-8 provide the minimum, average and maximum samples that can be extracted for each device using the selected 13 minute sub-window. It can be seen that in all datasets but REFIT, there are devices for which no training example can be generated while the maximum number of samples differ by orders of magnitude, from hundreds in REDD and IAWA to tens of thousands in UK-DALE and REFIT. After the cleaning and sub-windowing, the GASF transformation was applied resulting in images of size  $100 \times 100$  pixels that subsequently need to be concatenated in strict order. Each image was also multiplied by the maximum value present in the transformed sub-window.

Finally the last column shows the number of appliance classes used in the final dataset after preprocessing and transformation, where certain appliance types were discarded due to low sample size (i.e. missing data). Based on empirical test presented later in Section VI, we excluded all appliance types that had less than 230 samples. By using domain knowledge, we also decided to treat appliances like fridge and freezer as the same type of device, since in its core they operate in the same way. Similar was done for toaster and kettle, since both devices use a similar heating element only the function of what is being heated is different, creating a new appliance type named heating element kitchen appliances (HEKA). This process resulted in only using 12 out of the available 53 appliances in UK-DALE, 11 out of 21 for ECO, 4 out of 17 for REDD, and 15 out of 23 for REFIT. Since IAWA is a small dataset, we allowed 81 samples for this case which led to keeping 4 out of 9 appliances.

### B. Model training and evaluation

For training, we shuffled each dataset and split it into a training and a test dataset in an 80:20 ratio. We performed the shuffle split three times and then trained the model on the training set and evaluated it on the test set of each dataset used separately. The results presented are averages of all shuffle split metrics results. Due to the imbalance of the datasets, we weighted the classes during the training process. The goal is to

TABLE III  
SUMMARY OF THE APPLIANCE MONITORING DATASETS USED IN THIS WORK.

Dataset	Sampl.	Time	Houses	Appliance	Min.	Avg.	Max.	Min. sampl.	Used
UK-DALE [27]	6s	4.3y	5	53	0	1596	15172	1986	12
ECO [28]	1s	8m	6	21	0	117	8580	236	11
REDD [29]	1s	several m <sup>1</sup>	6	17	0	88	582	275	4
Iawe [30]	1s	73d	1	9	0	183	747	81	4
REFIT [31]	8s	2y	20	23	71	12873	72600	289	15

<sup>1</sup> Authors claim they collected the data through several months but did not provide an exact number

penalize misclassification by the minority classes by setting a higher class weight while reducing the weight for the majority class. The weights were assigned inversely proportional to the proportion of the class in the dataset, i.e., the classes with the lowest proportion were assigned the highest weight and those with the highest proportion were assigned the lowest weight. The backbone models were trained for 150 epochs and batch size 32, while the TL model was trained for 50 epochs with the same batch size.

For performance evaluation we use the standard metrics precision, recall and F1 score for each class. The metrics are expressed as: Precision =  $\frac{TP}{TP+FP}$ , Recall =  $\frac{TP}{TP+FN}$ , and F1-score =  $\frac{2 \times \text{Precision} \times \text{Recall}}{\text{Precision} + \text{Recall}}$  where TP, FP and FN stand for true positives, false positives and false negatives.

### C. Determining the number of classes and samples needed for transfer learning

To analyze how the number of classes in a dataset used for training a backbone model affects the TL process, a multitude of backbone models were trained, each with a different number of classes present in the subset of training dataset. Since REFIT dataset has the highest number of different classes this was used as the main dataset for generating the subset training datasets. For each subset, the classes were selected at random. The first subset contained two different classes and then, with each iteration, we increased the number of randomly selected appliance types by one until all of the 15 classes was used. Each trained backbone model was then used in the architecture presented in Section IV a and evaluated on the subset of ECO dataset for faster testing. For each iteration an average F1 was recorded.

We also analyzed how the number of positive samples of each class affects the backbone training process. Twelve experiments were conducted, where the number of samples for each class was increasing from 50 to 550 samples with a step of 50. Each backbone model was trained using the architecture presented in Section IV a and evaluated according to methodology presented in Section V b and an average F1 score was recorded. We were mostly interested in the smallest number of samples needed to train a useful backbone model. For plotting the results and approximating the recorded discrete values, the Savitzky–Golay filter was used with 1st order polynomials and window length of 3.

## VI. RESULTS

In this section, we evaluate the relative performance and computational complexity of the proposed feature expansion

approach proposed in Section III and designed model proposed in Section IV for solving the (N)ILM classification problem formulated in Section II. The experimental details used to obtain the results are detailed in Section V.

The results for each dataset are presented in Tables IV–VIII where the first column lists the classes ( $C_i$ ), while the remaining columns list the selected metrics of the trained models. **In the last column we list the number of samples present in the training and testing sets in model training.** The last row of each table is reserved for the weighted averages of the selected metrics, that compensates for the unbalanced representation of classes and thus enables easier comparison between the results of different methods and datasets.

### A. Comparison of the backbone model to imaging baseline

From Table IV, it can be seen that the proposed model performs with an F1 score starting from 0.90 for most of the classes selected in UK-DALE. In terms of F1 score, our proposed method outperforms the baseline VGG11 method by up to 0.18, except HEKA and microwaves. According to the weighted average of the F1 score, our method overall outperforms the VGG11 by 0.06. Since the computer monitor and desktop computers have a similar pattern and can be easily confused by the models, it can be seen from the table that our method significantly improves upon the results of the baseline model with a difference in F1 score of up to 0.18.

It can be seen from the last row of Table V that in terms of weighted average F1 score, our method is slightly worse compared to the VGG11 baseline model. Although the baseline model outperforms our model for five out of eleven classes, the performance difference is not significant, with the exception of the lamp class. For the lamp class, our model performs with an F1 score of 0.67 compared to 0.85 for the baseline model. At the same time, we can see that our model significantly outperforms the baseline in detecting the microwave class with an F1 score greater by 0.25 and broadband router class that has an F1 score greater by 0.32 which might indicate a superior ability to detect appliances with a short working cycle.

The performance of the model on the REDD dataset, that is smaller than the previous two, can be found in Table VI. In terms of the weighted average F1 score, the baseline model slightly outperforms our proposed model by 0.03. Similar to the ECO dataset, the proposed model is not significantly worse at detecting appliances, with the exception of the microwave class where it considerably outperforms the baseline model.

TABLE IV  
UKDALE CLASSIFICATION RESULTS

Class	Proposed model			baseline VGG11			baseline TS FCN			baseline TS ResNet			Num. samp.	
	Prec.	Rec.	F1	Prec.	Rec.	F1	Prec.	Rec.	F1	Prec.	Rec.	F1	Train	Test
HEKA	0.95	0.87	0.90	0.89	0.93	0.91	0.82	0.25	0.38	0.72	0.24	0.37	7834	1959
fridge/freezer	0.99	0.97	0.98	0.96	0.97	0.96	0.97	0.65	0.78	0.79	0.11	0.20	5997	1499
HTPC	0.93	0.95	0.94	0.75	0.80	0.77	0.73	0.15	0.25	0.25	0.19	0.22	2400	600
boiler	0.97	0.97	0.97	0.92	0.91	0.91	0.81	0.79	0.80	0.88	0.83	0.85	2862	715
computer monitor	0.88	0.93	0.90	0.72	0.72	0.72	0.54	0.52	0.53	0.63	0.40	0.49	3338	835
desktop computer	0.92	0.96	0.94	0.80	0.75	0.77	0.79	0.37	0.50	0.88	0.36	0.52	2677	669
laptop computer	0.99	0.97	0.98	0.91	0.91	0.91	0.87	0.88	0.88	0.62	0.92	0.74	3925	981
light	0.97	0.98	0.98	0.90	0.84	0.87	0.35	0.84	0.50	0.34	0.87	0.49	2400	600
microwave	0.78	0.90	0.84	0.88	0.89	0.89	0.87	0.09	0.16	0.90	0.10	0.19	4184	1046
server computer	0.98	0.96	0.97	0.95	0.95	0.95	0.32	0.73	0.45	0.11	0.17	0.14	1589	397
television	0.96	0.90	0.93	0.82	0.81	0.81	0.51	0.47	0.48	0.54	0.33	0.41	4163	1041
washer dryer	0.97	0.99	0.98	0.93	0.91	0.92	0.40	0.93	0.56	0.63	0.96	0.76	2215	554
Weighted avg.	<b>0.94</b>	<b>0.94</b>	<b>0.94</b>	0.88	0.88	0.88	0.69	0.53	0.59	0.62	0.46	0.52		

TABLE V  
ECO CLASSIFICATION RESULTS

Class	Proposed model			baseline VGG11			baseline TS FCN			baseline TS ResNet			Num. samp.	
	Prec.	Rec.	F1	Prec.	Rec.	F1	Prec.	Rec.	F1	Prec.	Rec.	F1	Train	Test
HEKA	0.99	0.98	0.99	0.93	0.97	0.95	0.47	0.47	0.47	0.01	0.05	0.02	586	146
fridge/freezer	0.99	0.95	0.97	0.99	0.98	0.98	0.90	0.86	0.88	0.96	0.72	0.82	15571	3893
HTPC	0.89	0.72	0.79	0.89	0.81	0.85	0.24	0.50	0.32	0.89	0.81	0.85	4691	1173
audio system	0.58	0.85	0.69	0.68	0.81	0.74	0.62	0.66	0.64	0.40	0.67	0.50	1104	276
broadband router	0.97	0.99	0.98	0.65	0.34	0.66	0.79	0.99	0.88	0.86	0.99	0.92	1257	314
coffee maker	0.86	1.00	0.92	0.93	0.91	0.92	0.53	0.76	0.62	0.73	0.50	0.59	261	65
computer	0.92	0.93	0.92	0.94	0.95	0.95	0.71	0.79	0.75	0.26	0.43	0.33	3358	839
lamp	0.54	0.87	0.67	0.83	0.87	0.85	0.30	0.28	0.29	0.17	0.01	0.02	862	216
laptop computer	0.74	0.90	0.81	0.79	0.88	0.83	0.46	0.27	0.34	0.43	0.68	0.53	2055	514
microwave	0.98	0.98	0.98	0.66	0.82	0.73	0.66	0.01	0.01	0.29	0.08	0.12	534	134
washing machine	1.00	0.94	0.97	0.81	0.86	0.83	0.98	0.34	0.50	0.27	0.36	0.31	189	47
Weighted avg.	0.92	0.90	0.91	<b>0.94</b>	<b>0.94</b>	<b>0.94</b>	0.67	0.60	0.63	0.62	0.55	0.58		

TABLE VI  
REDD CLASSIFICATION RESULTS

Class	Proposed model			baseline VGG11			baseline TS FCN			baseline TS ResNet			Num. samp.	
	Prec.	Rec.	F1	Prec.	Rec.	F1	Prec.	Rec.	F1	Prec.	Rec.	F1	Train	Test
fridge/freezer	0.76	0.92	0.83	0.89	0.93	0.91	0.80	0.87	0.83	0.99	0.86	0.92	583	146
electric furnace	0.77	0.86	0.81	0.85	0.92	0.88	0.27	0.86	0.41	0.54	0.93	0.68	370	92
light	0.82	0.72	0.77	0.81	0.80	0.81	0.77	0.37	0.50	0.83	0.66	0.74	1401	351
microwave	0.78	0.95	0.85	0.49	0.71	0.58	0.13	0.29	0.18	0.19	0.35	0.25	220	55
sockets	0.75	0.72	0.74	0.81	0.73	0.76	0.63	0.40	0.49	0.69	0.59	0.64	1373	343
Weighted avg.	0.78	0.78	0.78	<b>0.82</b>	<b>0.81</b>	<b>0.81</b>	0.62	0.48	0.54	0.72	0.65	0.67		

TABLE VII  
IAWE CLASSIFICATION RESULTS

Class	Proposed model			baseline VGG11			baseline TS FCN			baseline TS ResNet			Num. samp.	
	Prec.	Rec.	F1	Prec.	Rec.	F1	Prec.	Rec.	F1	Prec.	Rec.	F1	Train	Test
air conditioner	1.00	1.00	1.00	1.0	0.87	0.93	0.94	0.99	0.96	1.0	0.99	0.99	135	34
computer	0.99	0.98	0.98	0.95	0.96	0.95	0.99	0.87	0.93	0.90	0.93	0.92	366	92
fridge/freezer	0.98	0.98	0.98	0.96	0.96	0.96	0.99	0.90	0.95	0.99	0.76	0.86	670	167
television	0.78	0.88	0.82	0.78	0.88	0.82	0.66	1.00	0.79	0.43	0.82	0.56	65	16
Weighted avg.	<b>0.98</b>	<b>0.97</b>	<b>0.97</b>	0.95	0.95	0.95	0.95	0.92	0.93	0.91	0.85	0.86		

TABLE VIII  
REFIT CLASSIFICATION RESULTS

Class	Proposed model			baseline VGG11			baseline TS FCN			baseline TS ResNet			Num. samp.	
	Prec.	Rec.	F1	Prec.	Rec.	F1	Prec.	Rec.	F1	Prec.	Rec.	F1	Train	Test
HEKA	1.00	0.99	1.00	0.89	0.86	0.87	0.78	0.89	0.84	0.29	0.05	0.09	24168	6042
fridge/freezer	0.98	0.97	0.97	0.91	0.92	0.91	0.90	0.95	0.92	0.98	0.88	0.93	39304	9826
audio system	0.40	0.89	0.55	0.38	0.43	0.40	0.31	0.66	0.42	0.17	0.82	0.28	1369	342
bread maker	0.90	1.00	0.95	0.62	0.72	0.66	0.99	0.40	0.56	0.94	0.46	0.62	254	64
broadband router	0.44	0.87	0.58	0.41	0.45	0.43	0.82	0.17	0.28	0.74	0.34	0.46	1803	451
computer	0.87	0.81	0.84	0.64	0.58	0.61	0.59	0.41	0.49	0.62	0.53	0.57	20574	5143
dehumidifier	0.66	0.95	0.78	0.74	0.69	0.70	0.79	0.74	0.71	0.13	0.67	0.22	490	123
dish washer	0.96	0.98	0.97	0.86	0.86	0.86	0.97	0.39	0.56	0.90	0.47	0.62	3133	783
electric space heater	0.71	0.88	0.78	0.61	0.60	0.60	0.48	0.09	0.15	0.04	0.08	0.07	747	187
food processor	0.77	0.95	0.85	0.70	0.65	0.68	1.00	0.02	0.04	0.27	0.43	0.33	702	175
pond pump	0.78	0.99	0.87	0.72	0.82	0.77	0.53	0.99	0.69	0.65	0.99	0.79	796	3186
television	0.91	0.82	0.86	0.75	0.76	0.75	0.49	0.60	0.54	0.57	0.61	0.59	31629	7908
tumble dryer	0.87	0.84	0.86	0.68	0.70	0.69	0.93	0.50	0.65	0.76	0.54	0.63	1203	301
washer dryer	0.69	0.59	0.64	0.30	0.34	0.32	0.92	0.29	0.45	0.53	0.43	0.48	231	58
washing machine	0.88	0.91	0.89	0.83	0.82	0.52	0.42	0.46	0.83	0.39	0.45	0.41	4011	1003
Weighted avg.	<b>0.92</b>	<b>0.91</b>	<b>0.91</b>	0.80	0.79	0.79	0.74	0.73	0.73	0.74	0.68	0.70		

The model detects the microwave class with an F1 score of 0.85 which is by 0.27 better than the baseline model. This is consistent with our observation that appliances with short working duration are in general easier to detect with our proposed method compared to the baseline.

The performance results for the IAWE, the smallest dataset, reflected in Table VII, show superior performance compared to the other datasets. According to the weighted average F1 score, our proposed method slightly outperforms the baseline model by 0.02, being better at detecting three out of four classes, and achieving the same F1 score as the baseline model in the detection of the television class.

The evaluation results for REFIT, the largest dataset, are shown in Table VIII. Compared to the baseline, our proposed model significantly outperform it by 0.12 according to the weighted averaged F1. Considering also the results in Table IV, a trend can be observed that our proposed method starts outperforming the baseline when the number of classes in the dataset increases, therefore having superior discrimination power. In terms of F1 score, our proposed method outperforms the baseline for every class of this dataset. An additional observation is that, in most cases, recall is much higher than precision for the proposed model, that can be explained by the unbalanced nature of the dataset and is subsequently taken into

account by the weighted average scores, where we can see that precision slightly outperforms the recall.

When we analyze the results of all datasets, we can see that our proposed method mainly improves the detection of appliances with short working duration such as microwave, HEKA, and others. The reason is that the baseline images are larger than those used in the video-like format. This degrades the resolution of the patterns, which can cause short power spikes to be easily missed by the VGG11 model. This shows that our method provides higher resolution while requiring only  $\approx 55\%$  of pixels needed by the images used in the baseline.

#### B. Comparison of the backbone model to the TS baseline

**A glance at the results of the both TS baseline models shows that our proposed model significantly outperforms the FCN and ResNet models. Similar it can be also said if the TS baseline models are compared to the VGG11 baseline. The reason for this is that both our proposed model and VGG11 model through the transformation better capture both spatial and temporal correlation between each pair of values from the time series. In general less complex FCN performs better than ResNet model on all datasets but REDD.**

From Table IV it can be seen that the proposed model with an F1 score from performs significantly better than the two TS baseline models. Looking at the weighted F1 score, it can be seen that our proposed model performs 0.35 better than the FCN baseline model and 0.42 better than the ResNet baseline model. Based on the microwave class, it can be seen that both models have problems especially in detecting short duration activity traces. A similar observation can be made for the other datasets.

Comparing weighted F1 score of our proposed model to the both TS baseline models for the ECO dataset in Table V it can again be seen that our proposed model significantly outperforms the TS baseline. Although not comparable to the performance of our model, it can be seen through the fridge/freezer and broadband router classes that in general the baseline models perform the best on traces that have a repetitive long term pattern.

In terms of weighted F1 score for REDD dataset in Table VI, our proposed method outperforms the baseline FCN by 0.24 and ResNet by 0.11. For example, on IAWF dataset in Table VII our model outperforms the FCN by just 0.04 and ResNet by 0.11. In general IAWF is also the best performing dataset for the TS baseline models. Similar to the previous two dataset, also here we can conclude that the the baseline models struggle the most with detection short activity duration appliance traces, while they have much less problems in detecting repetitive pattern traces.

Finally, the comparison of our proposed method to the baseline on the REFIT dataset can be seen in the Table VIII. Again, comparing the weighted F1 scores, our model outperforms the baseline FCN and ResNet models by up to 0.21. Similar observations can be made as for the other datasets. Due to better capturing of the time correlations between the time steps within a trace, our model can better detect appliances with shorter duration of activity, such as HEKA. In general our proposed method, and also baseline imaging method, significantly outperform the raw TS baseline with the state of the art architecture. Although, the computational complexity of our proposed model is higher then both baseline TS models, the performance boost we get with sub-window imaging is providing a better ratio between the computational complexity and performance compared to the baseline TS models.

### C. Analysis of samples and classes needed for successful backbone training process

Figure 5 presents the effect of the number of samples on backbone training process. It can be seen from the graph that the average F1 score steadily rises with the increase of the number of samples. The elbow of the curve shows at around 150 samples where the F1 score is around 0.70. Performing and evaluating the transfer learning, we selected the minimum number of samples per class at 230 aiming for an F1 score around 0.75.

In Figure 6 the effect that the number of different classes have on TL is presented. The elbow curve occurs between 5 and 6 classes which results in an average F1 score between

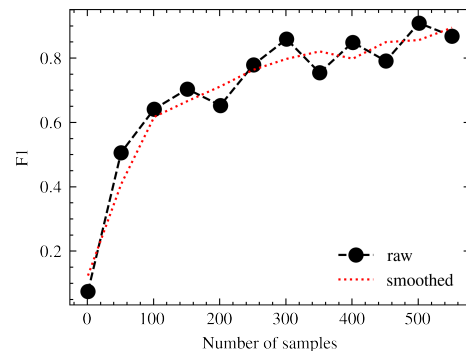


Fig. 5. Effect of selected number of samples in the dataset on the average F1 score of TL

0.70 and 0.75. What can also be observed is that the average F1 score steadily increases with the number of different devices present in the dataset. This shows that with the increase in diversity and number of devices, the trained model can extract more general features from the data which can then be easier applied to unseen cases in other datasets.

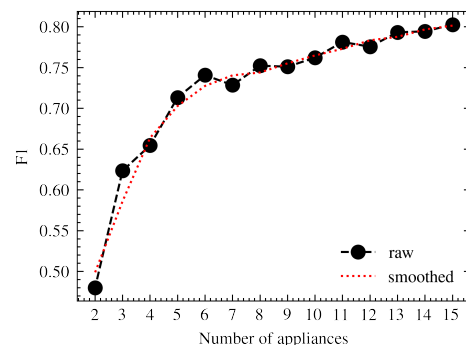


Fig. 6. Effect of selected number of appliances in the backbone model on the average F1 score of TL

### D. Evaluating the transfer learning model

According to the experimental results in Section VI-C, which shows how important the number of different classes is for the classification performance of a model, the model trained on REFIT was chosen for the backbone of our TL model because it had the highest number of classes used in training, while it performed with a similar F1 score as the models trained on UK-DALE and ECO. **The number of samples present in the training and testing sets is the same as with training the models from scratch.**

**Given the increasing popularity of modern loads to combat global climate change, we wanted to see if our proposed TL method could detect photovoltaic panels. To test this, we collected two days of power data from our local photovoltaic array at a sampling rate of 6s. We then randomly selected one appliance from each dataset used in the TL experiments and created a new training dataset, which was then transformed and processed according to the dataset preparation methodology presented in Section V.**

TABLE IX  
TL RESULTS ON SELECTED DATASETS

Dataset	Class	Refit backbone model		
		Prec.	Rec.	F1
UK-DALE	HEKA	0.88	0.78	0.83
	fridge/freezer	0.94	0.92	0.93
	HTPC	0.77	0.81	0.79
	boiler	0.88	0.89	0.89
	computer monitor	0.81	0.75	0.77
	desktop computer	0.77	0.84	0.80
	laptop computer	0.98	0.90	0.94
	light	0.79	0.90	0.84
	microwave	0.66	0.80	0.72
	server computer	0.80	0.93	0.86
	television	0.88	0.84	0.86
washer dryer	0.95	0.93	0.94	
	Weighted avg.	0.85	0.85	0.85
ECO	HEKA	0.99	0.97	0.98
	fridge/freezer	0.98	0.78	0.87
	HTPC	0.71	0.46	0.56
	audio system	0.52	0.74	0.61
	broadband router	0.45	0.85	0.58
	coffee maker	0.57	0.94	0.71
	computer	0.84	0.71	0.77
	lamp	0.22	0.65	0.32
	laptop computer	0.53	0.73	0.62
	microwave	0.78	0.97	0.87
	washing machine	0.39	0.96	0.56
	Weighted avg.	0.82	0.73	0.75
REDD	fridge/freezer	0.68	0.91	0.78
	electric furnace	0.61	0.86	0.71
	light	0.79	0.71	0.75
	microwave	0.81	0.95	0.87
	sockets	0.78	0.64	0.70
	Weighted avg.	0.75	0.74	0.74
IAWE	air conditioner	1.00	1.00	1.00
	computer	0.99	0.96	0.97
	fridge/freezer	0.98	0.92	0.95
	television	0.50	0.94	0.65
		Weighted avg.	0.96	0.94
Own	photovoltaic	0.66	0.98	0.79
	broadband router	0.91	0.95	0.93
	computer monitor	0.97	0.84	0.90
	fridge/freezer	0.74	0.96	0.84
	microwave	0.65	0.53	0.58
	Weighted avg.	0.89	0.83	0.85

The first twelve rows of the Table IX show the results of transferring the backbone model to UK-DALE. In general, it is evident that the model performs with a weighted F1 score of 0.85, which is by 0.09 worse than the model trained from scratch in Table IV. Compared to Table IV, the highest performance drop in terms of F1 score can be observed for the desktop computer and light classes, both of them dropping their F1 score by 0.14, while the laptop computer and washer dryer classes are performing worse by only 0.04.

The next eleven rows of the Table IX, show the results of the transferred ECO classifier. According to the weighted F1 score, ECO performs worse by 0.16 compared to the ECO model trained from scratch. Here the worst F1 score can be observed for the broadband router, 0.40, and washing machine class with an F1 drop of 0.41. The best performing class is HEKA which performs with only 0.01 worse F1 score compared to the results in Table V.

The TL model performance for the REDD dataset can be found in the next six rows under the ECO dataset results in Table IX. In general, the performance of the TL model in terms of weighted F1 score is 0.04 worse than that of the model trained from scratch. The model performs best in detecting the microwave class with an F1 score of 0.87 which is by 0.02 better than the model trained from scratch in Table VI. The highest drop, compared to the F1 score in Table VI, can be seen for the electric furnace class which is worse by 0.10. All the remaining classes also perform worse, but their F1 score drop ranges between 0.02 for light and 0.05 for the fridge/freezer class.

Next five rows refer to the IAWE dataset TL model performance results as listed in Table IX. The general observation is that the TL model again achieves the highest weighted average F1 results among all the selected datasets. The model achieves a weighted average F1 score of 0.95, which is 0.02 lower than the model trained from scratch in Table VII. The model is able to classify the air conditioner class with a perfect F1 score of 1.00 which is the same as for the model trained from scratch. In terms of F1 score, both the computer and fridge/freezer classes perform slightly worse than in Table VII with the drop being 0.01 and 0.03, respectively. The classification of the television class is the worst with an F1 score of 0.65, which is by 0.17 worse than in Table VII. **Additionally, it can be seen that the TL model also significantly outperforms both baseline TS models. This further emphasises the benefits of our proposed transformation.**

The last five rows in the Table IX show our custom made dataset to test whether our proposed TL method can classify photovoltaic modules. Based on the F1 score of 0.79, it can be seen that the TL method can successfully detect photovoltaic modules among other appliances. Precision of both photovoltaic and microwave classes is lower compared to others. This was due to the unstable weather conditions when the photovoltaic data was collected, so the power output and pattern of photovoltaic was similar to microwaves in some cases. In general, the TL method performed with an F1 score of 0.85.

The results show that training a feature extraction model can help simplify model development for the BEMS system with

the process of transfer learning. Although all four datasets experienced a performance drop compared to the models trained from scratch, the performance was still within acceptable range especially considering it takes 3 times less epochs to train such model. [14] reported in their paper a drop in precision of about 28 percentage points when transferring the model to unseen device types. In our case, four out of five classes in the dataset REDD are not part of the dataset REFIT and the precision drop for these classes was up to 16 percentage points, so compared to [14], our precision drop is up to 12 percentage points lower.

#### E. Trade-off analysis for computational complexity

As mentioned in the Section I-A4 DL model computational complexity of TS to image transformation methods is their major limitation, especially compared to raw TS DL models. To understand the computational complexity trade-offs of the DL model using the proposed sub-windowed GAF representation compared to the state-of-the-art GAF image transformation and the raw TS model, we performed two different comparisons based on the equations presented in Section IV-A.

1) *FLOPs per convolutional layer of sub-windowed GAF vs SotA GAF*: The first comparison uses a convolutional layer, where we calculate the number of FLOPs required for a convolution of a TS sample transformed by both our proposed method and the state-of-the-art GAF using Eq. 7. To make the computation as simple as possible we assume that the convolutional layer has a single kernel of size  $k \times k$  and padding of size  $\frac{k}{2}$ . Additionally, we assume the input channel  $C = 1$ . This simplifies Eq. 7 to:

$$FLOPs = R \times W \times W \times (k \times k + 1) \quad (11)$$

$$FLOPs_{proposed} = 5 \times 120 \times 120 \times (7 \times 7 + 1) \quad (12)$$

$$= 3.6 \text{ MFLOPs} \quad (13)$$

$$FLOPs_{GAF} = 1 \times 600 \times 600 \times (7 \times 7 + 1) \quad (14)$$

$$= 18 \text{ MFLOPs} \quad (15)$$

We fix the kernel size  $k \times k = 7 \times 7$ , consider  $N = 600$ ,  $W = 120$  resulting in  $R = 5$  sub-window GAF images of shape  $M = 120 \times 120$ . State-of-the-art GAF uses the transformation window  $W = N = 600$ , resulting in  $R = 1$  images of shape  $M = 600 \times 600$ . With these design choices, it can be seen that  $FLOPs_{proposed} = 3.6$  MFLOPs and  $FLOPs_{GAF} = 18$  MFLOPs, resulting in a 5-time improvement for the proposed model per convolution layer. Corroborated with the discrimination performance evaluated in the previous subsections, this result makes the proposed model a preferred option for dimensionality expansion.

2) *FLOPs vs input tensor size*: In the second comparison, we investigate how the computational complexity of the model architectures presented in Section IV scales with the size of the model input. The purpose of this comparison is to estimate how sub-window GAF, state-of-the-art GAF, and raw TS shapes of input affect their corresponding

models. The FLOPs were calculated according to the guidelines presented in Section IV-A and listed in Table X where each line first contains the size for  $H$  followed by the model complexity in GFLOPs.

TABLE X  
DL FLOPs OF THE MODELS FROM SECTION IV FOR DIFFERENT SIZES OF THE INPUT TENSOR  $H_{[R \times W \times W]}$ .

Input/ Model [GFLOPs]	Rx(WxW)	Rx(WxW)	Rx(WxW)
Sub-window imaging/ proposed model	1x(100x100) ≈0.58	3x(100x100) ≈1.75	6x(100x100) ≈3.50
Image (SotA GAF)/ VGG11	1x(100x100) ≈1.5	1x(300x300) ≈13.3	1x(600x600) ≈54.6
raw TS/ FCN	100x(1x1) ≈0.026	300x(1x1) ≈0.08	600x(1x1) ≈0.16
raw TS/ ResNet	100x(1x1) ≈0.05	300x(1x1) ≈0.14	600x(1x1) ≈0.29

As can be seen from the first line, the computational complexity of our proposed method scales linearly. By keeping the  $W = 100$  and increasing  $R \in \{1, 3, 6\}$ , the complexity increases to 0.58, 1.75 and 3.50 respectively. The same can be observed for the two TS models FCN and ResNet in lines 4 and 5 of the table. However, if we look at the third row, where the results for the state-of-the-art GAF are presented, it can be seen that the computational complexity increases quadratically with input size of  $600 \times 600 \times 1$  needing approximately 54.6 GFLOPs for one forward pass. This complexity increase is also the reason why the majority of state of the art architectures, such as AlexNet, VGG11 to 19, Inception and image ResNet, are trained in the literature on images of size up to  $300 \times 300$  pixels.

The results in Table X highlight the limitation of the state-of-the-art GAF approach, which becomes too expensive beyond a certain point to be a viable solution for time series analysis, and highlight the advantage of the proposed sub-window GAF transformation.

## VII. CONCLUSION

In this paper we proposed a *new approach* for appliance classification that has several computational advantages over the state of the art while also showing better performance. The novelty consists of a *new dimensionality expansion* technique of the time series to sub-window GAF and a *tailored deep neural network*. We also elaborated on guidelines for tailoring the deep neural network to be resource aware and analysed the computational complexity of appliance classification approaches for the proposed, state-of-the-art GAF and raw TS approaches.

Our experiments show that the proposed approach is able to classify household appliances with an average F1 score of 0.88 across open datasets containing 29 appliances. Our method yields similar performance while requiring only  $\approx 55\%$  of pixels needed by the state of the art image transformation models. In addition to being much more computationally efficient compared to the images, the proposed method also significantly outperforms both state-of-the-art TS architectures.

We then studied the suitability of the proposed method for faster model development through *cross-dataset intra-domain transfer learning*. We found that the proposed transfer learning approach performs with an average F1 score of 0.80, while requiring only a third of training epochs compared to training a model from scratch. We also show that 230 samples of data per class is enough that the model can be transferred to a new building with an F1 score of 0.75. We also found that the model it improves the precision drop for unseen devices by up to 12 percentage points compared to the state of the art.

#### ACKNOWLEDGEMENTS

This work was funded by the Slovenian Research Agency under the Grant P2-0016.

#### REFERENCES

- [1] X. Fang, S. Misra, G. Xue, and D. Yang, "Smart grid — the new and improved power grid: A survey," *IEEE Communications Surveys Tutorials*, vol. 14, no. 4, pp. 944–980, 2012.
- [2] M. Zhuang, M. Shahidehpour, and Z. Li, "An overview of non-intrusive load monitoring: Approaches, business applications, and challenges," in *2018 International Conference on Power System Technology (POWERCON)*, 2018, pp. 4291–4299.
- [3] D. Lee and C.-C. Cheng, "Energy savings by energy management systems: A review," *Renewable and Sustainable Energy Reviews*, vol. 56, pp. 760–777, 2016. [Online]. Available: <https://www.sciencedirect.com/science/article/pii/S1364032115013349>
- [4] M. Hazas, A. Friday, and J. Scott, "Look back before leaping forward: Four decades of domestic energy inquiry," *IEEE pervasive Computing*, vol. 10, no. 1, pp. 13–19, 2010.
- [5] B. Neenan, J. Robinson, and R. Boisvert, "Residential electricity use feedback: A research synthesis and economic framework," *Electric Power Research Institute*, vol. 3, pp. 123–129, 2009.
- [6] E. Gomes and L. Pereira, "Pb-nilm: Pinball guided deep non-intrusive load monitoring," *IEEE Access*, vol. 8, pp. 48 386–48 398, 2020.
- [7] C. Zhang, M. Zhong, Z. Wang, N. Goddard, and C. Sutton, "Sequence-to-point learning with neural networks for non-intrusive load monitoring," in *Proceedings of the AAAI conference on artificial intelligence*, vol. 32, no. 1, 2018.
- [8] M. D’Incecco, S. Squartini, and M. Zhong, "Transfer learning for non-intrusive load monitoring," *IEEE Transactions on Smart Grid*, vol. 11, no. 2, pp. 1419–1429, 2020.
- [9] T.-T.-H. Le and H. Kim, "Non-intrusive load monitoring based on novel transient signal in household appliances with low sampling rate," *Energies*, vol. 11, no. 12, 2018. [Online]. Available: <https://www.mdpi.com/1996-1073/11/12/3409>
- [10] T.-T.-H. Le, J. Kim, and H. Kim, "Classification performance using gated recurrent unit recurrent neural network on energy disaggregation," in *2016 International Conference on Machine Learning and Cybernetics (ICMLC)*, vol. 1, 2016, pp. 105–110.
- [11] J. Kelly and W. Knottenbelt, "Neural nilm: Deep neural networks applied to energy disaggregation," ser. BuildSys ’15. New York, NY, USA: Association for Computing Machinery, 2015, p. 55–64. [Online]. Available: <https://doi.org/10.1145/2821650.2821672>
- [12] O. Krystalakos, C. Nalmpantis, and D. Vrakas, "Sliding window approach for online energy disaggregation using artificial neural networks," in *Proceedings of the 10th Hellenic Conference on Artificial Intelligence*, ser. SETN ’18. New York, NY, USA: Association for Computing Machinery, 2018. [Online]. Available: <https://doi.org/10.1145/3200947.3201011>
- [13] R. Bonfigli, A. Felicetti, E. Principi, M. Fagiani, S. Squartini, and F. Piazza, "Denoisising autoencoders for non-intrusive load monitoring: Improvements and comparative evaluation," *Energy and Buildings*, vol. 158, pp. 1461–1474, 2018. [Online]. Available: <https://www.sciencedirect.com/science/article/pii/S0378778817314457>
- [14] Z. Zhou, Y. Xiang, H. Xu, Z. Yi, D. Shi, and Z. Wang, "A novel transfer learning-based intelligent nonintrusive load-monitoring with limited measurements," *IEEE Transactions on Instrumentation and Measurement*, vol. 70, pp. 1–8, 2021.
- [15] Y. Liu, X. Wang, and W. You, "Non-intrusive load monitoring by voltage-current trajectory enabled transfer learning," *IEEE Transactions on Smart Grid*, vol. 10, no. 5, pp. 5609–5619, 2019.
- [16] L. De Baets, J. Ruysinck, C. Develder, T. Dhaene, and D. Deschrijver, "Appliance classification using vi trajectories and convolutional neural networks," *Energy and Buildings*, vol. 158, pp. 32–36, 2018. [Online]. Available: <https://www.sciencedirect.com/science/article/pii/S0378778817312690>
- [17] G. Hart, "Nonintrusive appliance load monitoring," *Proceedings of the IEEE*, vol. 80, no. 12, pp. 1870–1891, 1992.
- [18] P. Bilski and W. Winiński, "The rule-based method for the non-intrusive electrical appliances identification," in *2015 IEEE 8th International Conference on Intelligent Data Acquisition and Advanced Computing Systems: Technology and Applications (IDAACS)*, vol. 1. IEEE, 2015, pp. 220–225.
- [19] M. Aiad and P. H. Lee, "Non-intrusive load disaggregation with adaptive estimations of devices main power effects and two-way interactions," *Energy and Buildings*, vol. 130, pp. 131–139, 2016.
- [20] O. Parson, S. Ghosh, M. Weal, and A. Rogers, "Non-intrusive load monitoring using prior models of general appliance types," in *Twenty-Sixth AAAI Conference on Artificial Intelligence*, 2012.
- [21] F. Paradiso, F. Paganelli, D. Giuli, and S. Capobianco, "Context-based energy disaggregation in smart homes," *Future Internet*, vol. 8, no. 1, 2016. [Online]. Available: <https://www.mdpi.com/1999-5903/8/1/4>
- [22] Y.-X. Lai, C.-F. Lai, Y.-M. Huang, and H.-C. Chao, "Multi-appliance recognition system with hybrid svm/gmm classifier in ubiquitous smart home," *Information Sciences*, vol. 230, pp. 39–55, 2013.
- [23] D. Weijßhaar, P. Held, S. Mauch, and D. Benyoucef, "Device classification for nilm using fit-ps compared with standard signal forms," in *2018 International IEEE Conference and Workshop in Öbuda on Electrical and Power Engineering (CANDO-EPE)*. IEEE, 2018, pp. 1–6.
- [24] J. Gao, E. C. Kara, S. Giri, and M. Berges, "A feasibility study of automated plug-load identification from high-frequency measurements," in *2015 IEEE global conference on signal and information processing (GlobalSIP)*. IEEE, 2015, pp. 220–224.
- [25] J. Kim, H. Kim *et al.*, "Classification performance using gated recurrent unit recurrent neural network on energy disaggregation," in *2016 international conference on machine learning and cybernetics (ICMLC)*, vol. 1. IEEE, 2016, pp. 105–110.
- [26] Q. Wu and F. Wang, "Concatenate convolutional neural networks for non-intrusive load monitoring across complex background," *Energies*, vol. 12, no. 8, 2019. [Online]. Available: <https://www.mdpi.com/1996-1073/12/8/1572>
- [27] J. Kelly and W. Knottenbelt, "The UK-DALE dataset, domestic appliance-level electricity demand and whole-house demand from five UK homes," *Scientific Data*, vol. 2, no. 150007, 2015.
- [28] C. Beckel, W. Kleiminger, R. Cicchetti, T. Staake, and S. Santini, "The eco data set and the performance of non-intrusive load monitoring algorithms," in *Proceedings of the 1st ACM conference on embedded systems for energy-efficient buildings*, 2014, pp. 80–89.
- [29] J. Z. Kolter and M. J. Johnson, "Redd: A public data set for energy disaggregation research," in *Workshop on data mining applications in sustainability (SIGKDD)*, San Diego, CA, vol. 25, no. Citeseer, 2011, pp. 59–62.
- [30] N. Batra, M. Gulati, A. Singh, and M. B. Srivastava, "It’s different: Insights into home energy consumption in india," in *Proceedings of the 5th ACM Workshop on Embedded Systems For Energy-Efficient Buildings*, 2013, pp. 1–8.
- [31] D. Murray, L. Stankovic, and V. Stankovic, "An electrical load measurements dataset of united kingdom households from a two-year longitudinal study," *Scientific data*, vol. 4, no. 1, pp. 1–12, 2017.
- [32] T. Kriechbaumer and H.-A. Jacobsen, "Blond, a building-level office environment dataset of typical electrical appliances," *Scientific data*, vol. 5, no. 1, pp. 1–14, 2018.
- [33] S. Makonin, F. Popowich, L. Bartram, B. Gill, and I. V. Bajić, "Ampds: A public dataset for load disaggregation and eco-feedback research," in *2013 IEEE electrical power & energy conference*. IEEE, 2013, pp. 1–6.
- [34] J. Gao, S. Giri, E. C. Kara, and M. Berges, "Plaid: A public dataset of high-resolution electrical appliance measurements for load identification research: Demo abstract," in *Proceedings of the 1st ACM Conference on Embedded Systems for Energy-Efficient Buildings*, ser. BuildSys ’14. New York, NY, USA: Association for Computing Machinery, 2014, p. 198–199. [Online]. Available: <https://doi.org/10.1145/2674061.2675032>
- [35] M. Kahl, A. ul Haq, T. Kriechbaumer, and H.-A. Jacobsen, "Whited-a worldwide household and industry transient energy data set," 2016.

- [36] A. Krizhevsky, I. Sutskever, and G. E. Hinton, “Imagenet classification with deep convolutional neural networks,” *Advances in neural information processing systems*, vol. 25, pp. 1097–1105, 2012.
- [37] Z. Zhao, P. Zheng, S. Xu, and X. Wu, “Object detection with deep learning: A review,” *IEEE Transactions on Neural Networks and Learning Systems*, vol. 30, no. 11, pp. 3212–3232, 2019.
- [38] A. Faustine and L. Pereira, “Improved appliance classification in non-intrusive load monitoring using weighted recurrence graph and convolutional neural networks,” *Energies*, vol. 13, no. 13, 2020. [Online]. Available: <https://www.mdpi.com/1996-1073/13/13/3374>
- [39] M. Mottahedi and S. Asadi, “Non-intrusive load monitoring using imaging time series and convolutional neural networks,” in *16th International Conference on computing in civil and building engineering*, 2016, pp. 705–710.
- [40] L. Kyrkou, C. Nalmpantis, and D. Vrakas, “Imaging time-series for nilm,” in *International Conference on Engineering Applications of Neural Networks*. Springer, 2019, pp. 188–196.
- [41] S. R. Tito, A. Ur Rehman, Y. Kim, P. Nieuwoudt, S. Aslam, S. Soltic, T. T. Lie, N. Pandey, and M. D. Ahmed, “Image segmentation-based event detection for non-intrusive load monitoring using gramian angular summation field,” in *2021 IEEE Industrial Electronics and Applications Conference (IEACon)*, 2021, pp. 185–190.
- [42] A. M. A. Ahmed, Y. Zhang, and F. Eliassen, “Generative adversarial networks and transfer learning for non-intrusive load monitoring in smart grids,” in *2020 IEEE International Conference on Communications, Control, and Computing Technologies for Smart Grids (SmartGrid-Comm)*, 2020, pp. 1–7.
- [43] E. Otovic, M. Njirjak, D. Jozinovic, G. Mauša, A. Micheleni, and I. Stajduhar, “Intra-domain and cross-domain transfer learning for time series data—how transferable are the features?” *Knowledge-Based Systems*, vol. 239, p. 107976, 2022. [Online]. Available: <https://www.sciencedirect.com/science/article/pii/S0950705121010984>
- [44] B. Bertalanič, M. Meža, and C. Fortuna, “Resource-aware time series imaging classification for wireless link layer anomalies,” *IEEE Transactions on Neural Networks and Learning Systems*, pp. 1–13, 2022.
- [45] M. Zhang, W. Wang, X. Liu, J. Gao, and Y. He, “Navigating with graph representations for fast and scalable decoding of neural language models,” *Advances in neural information processing systems*, vol. 31, 2018.
- [46] K. Simonyan and A. Zisserman, “Very deep convolutional networks for large-scale image recognition,” *arXiv preprint arXiv:1409.1556*, 2014.
- [47] H. A. Dau, A. Bagnall, K. Kamgar, C.-C. M. Yeh, Y. Zhu, S. Gharghabi, C. A. Ratanamahatana, and E. Keogh, “The ucr time series archive,” *IEEE/CAA Journal of Automatica Sinica*, vol. 6, no. 6, pp. 1293–1305, 2019.
- [48] Z. Wang, W. Yan, and T. Oates, “Time series classification from scratch with deep neural networks: A strong baseline,” in *2017 International Joint Conference on Neural Networks (IJCNN)*, 2017, pp. 1578–1585.
- [49] N. Batra, J. Kelly, O. Parson, H. Dutta, W. Knottenbelt, A. Rogers, A. Singh, and M. Srivastava, “Nilmtk: An open source toolkit for non-intrusive load monitoring,” in *Proceedings of the 5th International Conference on Future Energy Systems*, ser. e-Energy '14. New York, NY, USA: Association for Computing Machinery, 2014, p. 265–276. [Online]. Available: <https://doi.org/10.1145/2602044.2602051>